Published in final edited form as:

Adv Healthc Mater. 2021 April ; 10(7): e2001706. doi:10.1002/adhm.202001706.

Cell-laden Gradient Hydrogel Scaffolds for Neovascularization of Engineered Tissues

Yusheng J. He,
Department of Surgery, University of Chicago, Address: 5841 S Maryland Ave, Suit E500, Chicago, IL 60637

Martin F. Santana,
Department of Biomedical Engineering, Illinois Institute of Technology, Address: 3255 South Dearborn Street, Suite 314, Chicago, IL 60616

Austeja Staneviciute,
Department of Biomedical Engineering, Illinois Institute of Technology, Address: 3255 South Dearborn Street, Suite 314, Chicago, IL 60616

Marja B. Pimentel,
Department of Biomedical Engineering, Illinois Institute of Technology, Address: 3255 South Dearborn Street, Suite 314, Chicago, IL 60616

Feipeng Yang,
Department of Biomedical Engineering, Illinois Institute of Technology, Address: 3255 South Dearborn Street, Suite 314, Chicago, IL 60616

Jacob Goes,
Department of Biomedical Engineering, Illinois Institute of Technology, Address: 3255 South Dearborn Street, Suite 314, Chicago, IL 60616

Keigo Kawaji,
Department of Biomedical Engineering, Illinois Institute of Technology, Address: 3255 South Dearborn Street, Suite 314, Chicago, IL 60616

Marcella Vaicik,
Department of Biomedical Engineering, Illinois Institute of Technology, Address: 3255 South Dearborn Street, Suite 314, Chicago, IL 60616

Rayan Abdulhadi,
Department of Biomedical Engineering, Illinois Institute of Technology, Address: 3255 South Dearborn Street, Suite 314, Chicago, IL 60616

Narutoshi Hibino,
Department of Surgery, University of Chicago, Address: 5841 S Maryland Ave, Suit E500, Chicago, IL 60637

yhe6@bsd.uchicago.edu, papavasiliou@iit.edu.

Supporting Information

Supporting Information is available from the Wiley Online Library or from the author.

Georgia Papavasiliou
Department of Biomedical Engineering, Illinois Institute of Technology, Address: 3255 South Dearborn Street, Suite 314, Chicago, IL 60616

Abstract

Gradients in mechanical properties, physical architecture and biochemical composition exist in a variety of complex tissues, yet 3D *in vitro* models that enable investigation of these cues on cellular processes, especially those contributing to vascularization of engineered tissues are limited. Here we report a photopolymerization approach to create cell-laden hydrogel biomaterials with decoupled and combined gradients in modulus, immobilized cell adhesive peptide (RGD) concentration and proteolytic degradation enabling spatial encapsulation of vascular spheroids to elucidate their impact on vascular sprouting in 3D culture. All vascular spheroids encapsulated in these gradient scaffolds exhibited spatial variations in total sprout length. Scaffolds presenting an immobilized RGD gradient promoted biased vascular sprouting toward increasing RGD concentration. Importantly, biased sprouting was found to be dependent on immobilized RGD gradient characteristics, including magnitude and slope, with increases in these factors contributing to significant enhancements in biased sprouting responses. Conversely, reduction in biased sprouting responses was observed in combined gradient scaffolds possessing opposing gradients in RGD and modulus. The presented work is the first to demonstrate the use of a cell-laden biomaterial platform to systematically investigate the role of multiple scaffold gradients as well as gradient slope, magnitude and orientation on vascular sprouting responses in 3D culture.

Keywords

Poly(ethylene glycol); Hydrogel; Gradient materials; Vascularization; Spheroid

1 Introduction

The inability to induce extensive and perfusable microvasculature within engineered tissues remains as a major hurdle to their clinical translation.[1–3] Cells and tissues located further than a few hundred microns from the nearest capillaries undergo hypoxia and apoptosis as oxygen transport beyond this distance becomes limited. Thus, the volume of tissue that can be engineered is restricted to the extent to which blood vessels can be stimulated to form within the implantable scaffold. One of the key goals of tissue engineering involves the design of biomaterial scaffolds of clinically relevant dimensions that can support the survival and growth of cell and tissue assembly *in vitro* and *in vivo*.

Various biomaterial strategies and techniques have been applied to induce neovascularization as a means for enhancing survival and functionality of engineered tissues. A common approach involves implantation of scaffolds which deliver neovascularization factors to stimulate recruitment of host vasculature.[4–9] In this approach, however, newly formed vessels are often limited to the periphery of the construct due to relatively slow vascular ingrowth, which compromises cellular and tissue viability within the scaffold interior.[10] An alternative approach involves encapsulation of endothelial and mural cell co-cultures within biomaterial scaffolds to form pre-vascularized tissues in vitro prior to implantation. This

strategy has been use to engineer pre-vascularized constructs that inosculate with host vasculature and induce perfusable and functional vessel formation following implantation.[1,11–13] The ability, however, to pre-vascularize complex tissues, including osteochondral, neural and renal tissues that possess spatial and temporal variations in mechanical properties, physical architecture and biochemical and cellular composition has yet to be achieved.[14–16] The native process of neovascularization requires that vascular cells respond to a variety of gradients provided by their surrounding extracellular matrix (ECM) which impact the direction, structure and rates of cell invasion and vascularized tissue remodeling. Therefore, the application of cell-laden gradient-based hydrogel platforms serve as important tools for screening vascular cell responses to physiologically relevant biochemical and mechanical spatiotemporal ECM cues in 3D culture that cannot be achieved using animal models.

The most commonly exploited approach for inducing vascularization of engineered tissues is through the design of scaffolds that present gradients of diffusible or immobilized growth factors.[17–20] Spatial variations of ECM proteins,[21,22] cell adhesion peptide ligands[23,24] as well as mechanical properties[25] have been shown to direct and enhance the migration of vascular cells highlighting the importance of these gradient cues on neovascularization. These studies, however, have focused on 2D cell responses to spatial variations of these signals, with cells seeded on the surface of gradient-based materials. Limited studies have explored the impact of these gradients on neovascularization in 3D culture. For example, collagen-based scaffolds presenting spatial variations in protein density and composition[26] or concentration gradients of hyaluronic acid (HA)[27] have been shown to induce directional migration of fibroblasts and biased vascular sprouting of embedded cell spheroids downstream of the HA gradient, respectively. The ECM is a dynamic microenvironment, that is continuously remodeled as a result of cell mediated proteolytic degradation during which mechanical properties, physical structure and biochemical composition vary both spatially and temporally. In addition, distinct tissue types differ in biochemical composition, stiffness and rates of proteolytic remodeling which collectively impact neovascularization; however, the role of spatial variations in these matrix properties on vessel assembly remains unclear.

In a previously published study we developed a free-radical photopolymerization approach, ascending frontal polymerization, to create proteolytically degradable poly(ethylene) glycol (PEG) hydrogels with continuous and decoupled gradients in elastic modulus and immobilized RGD cell adhesion peptide ligands.[28] Specifically, scaffolds with linear gradients in modulus and immobilized RGD concentration were produced using visible light free-radical photopolymerization in which precursor solutions of varying composition were fed by programmable syringe pumps to form a localized ascending photopolymerizable hydrogel front. The scaffold fabrication process in our previous study was not designed for the generation of cell-laden gradient scaffolds. Thus, the novelty of our current photopolymerization process lies in the ability to create cell-laden scaffolds which physically and spatially entrap vascular co-culture spheroids along the gradient, which to our knowledge has not been previously attempted. Cell-laden gradient-based approaches, such as the one used in our study, are highly useful for a variety of cellular-based therapies such as those that require scaffolds to deliver cells upon implantation.[29] In the present study, we

adjusted co-initiator concentration and optimized the scaffold fabrication process to regionally encapsulate cellular spheroids during ascending frontal photopolymerization. Utilizing this cell-laden gradient hydrogel fabrication approach we engineered scaffolds with decoupled and combined spatial variations in elastic modulus, proteolytic degradation and immobilized RGD concentration and tuned gradient characteristics including gradient magnitude, slope, and orientation. Specifically, hydrogel scaffolds comprised of (1) steep and (2) shallow gradient slopes in immobilized RGD with uniform modulus and protease-sensitivity, (3) gradients in elastic modulus with uniform RGD concentration and protease-sensitivity, (4) gradients in protease-sensitivity with uniform RGD concentration and modulus, and (5) a combined gradient scaffold possessing concurrent RGD and protease-sensitivity gradients and an opposing modulus gradient were created using ascending frontal polymerization. We hypothesized that the selected combined gradient scaffold would induce prominent spatial variations in vascular spheroid responses in 3D culture. This hypothesis was supported by our recently published study focused on full factorial screening and design of experiments (DOE) analysis in isotropic PEG scaffolds which revealed an optimized combination whereby increases in proteolytic scaffold degradation rate and immobilized RGD concentration result in synergistic enhancements in vascular sprouting in 3D culture.[30] Although gradients in immobilized biochemical cues, including growth factor and adhesion protein composition on vascular cell behavior have been have previously explored, effects of spatial variations in proteolytic degradation on vascular sprouting responses, to our knowledge, have not been previously investigated and are critical mediators of cell migration and vascularized tissue remodeling rates. In the present study gradient properties were tuned by manipulating the spatial concentration of PEG macromers including: PEG diacrylate (PEGDA) cross-linkers containing (1) one (SSite) or (2) two (DSite) MMP-sensitive peptide cleavage sites, (3) an RGD-containing PEG monoacrylate macromer (RGD-PEGMA) and (4) a non-functional PEG monoacrylate macromer (PEGMA) as shown in Figure 1. To understand the impact of gradient types and characteristics on 3D vascular sprouting responses in culture, we evaluate the vascular sprouting response of co-culture spheroids comprised of human umbilical vein endothelial cells (HU-VECs) and human arterial smooth muscle cell (HUASMC) to the scaffold gradients by encapsulating them along the imposed gradients at different region during photopolymerization as shown in Figure 2. The presented approach provides a robust tunable in vitro platform for screening various physiologically relevant gradients on neovascularization responses and for creation of complex engineered tissues with spatial heterogeneity in biochemical cues and material properties.

2 Results

2.1 RGD gradients lead to biased vascular sprouting

Hydrogel scaffolds containing immobilized RGD concentration gradients were created by gradually changing the molar ratio of RGD-PEGMA to PEGMA in the precursor feed while keeping the total concentrations of monoacrylate macromers and PEGDA crosslinker(DSite) constant in the precursor solution fed to the reaction vessel over time. The magnitude and slope of the gradient was modulated by varying the macromer concentration gradient profile into the precursor feed stream using a programmable syringe pump. As a result, scaffolds

with linear, steep gradients (gradient slope of 322±31 μM/mm, R^2 = 0.89) in immobilized RGD concentration ranging from 0.75 to 3.43 mM over a scaffold length of 10mm were created.. Scaffolds with linear, shallow gradients (gradient slope of 160±15 μM/mm, R^2 = 0.92) in immobilized RGD concentration ranging from 0.37 to 1.71 mM over a scaffold length of 10 mm (Figure 3A) were also fabricated. The elastic modulus of both steep and shallow RGD gradient hydrogels remained relatively uniform at 4035±275 Pa and 3943±233 Pa, respectively. The proteolytic susceptibility of the scaffold was quantified by measuring hydrogel degradation kinetics along the gradient as described above in enzyme solution. Both steep and shallow RGD gradient hydrogels exhibited uniform degradation kinetics as expected with complete material degradation occurring after a 24-hour incubation in collagenase solution (Figure 3B, 3C, and 3D). To summarize, hydrogels with varying gradient slopes in immobilized RGD were created using ascending frontal polymerization while maintaining a uniform modulus and scaffold degradation rate.

A co-culture model of sprouting angiogenesis was used to investigate the effect of the imposed matrix gradients on 3D vascular sprout formation. Cell spheroids were embedded within gradient scaffolds at three distinct regions (top, middle and bottom) along the imposed gradient(s). Within each gradient hydrogel, the spheroids were exposed to the same gradient slope, but different gradient magnitudes. The approximations of the local matrix properties of each region of the gradient scaffolds are summarized in the supplementary data section(Table S1.)To determine the cell type leading the invasion and sensing the imposed gradient(s), spheroids were stained with the nuclear F-actin marker phalloidin and an endothelial cell marker UEA I. Confocal images of stained sprouts indicate that the tips of sprouts are composed of endothelial cells suggesting that sprout invasion is led by endothelial cells (Figure S1). Acquired confocal images of vascular sprouts and quantification of sprout length by angle within steep RGD gradient scaffolds indicated that spheroids embedded in scaffold regions closest to the gradient(top and middle) exhibited significant preferential sprouting responses towards increasing RGD concentration (−45°,0°and 45°) at both days 7 and 14 (Figure 3 E–M). Conversely, spheroids positioned in scaffold regions furthest from the gradient (bottom) exhibited minimal and unbiased sprouting. Increases in vascular sprout outgrowth from day 7 to day 14 were observed in the top and middle regions of the scaffold. In contrast, scaffolds possessing shallow gradients in immobilized RGD resulted in decreases in overall sprouting and biased sprout formation (Figure 3 N–V). Nonetheless, spheroids embedded in the top and middle regions of the shallow RGD gradient hydrogel scaffolds exhibited biased sprouting towards increasing RGD concentration (−45°,0°and 45°) by day 14.

2.2 Modulus gradient induce spatial variations in vascular sprouting

Hydrogel scaffolds embedded with gradients in elastic modulus were created by gradually increasing the SSite PEGDA crosslinker concentration while keeping the RGD-PEGMA concentration constant in the precursor solution fed into reaction vessel over time. As a result, the elastic modulus increased linearly from 1054 to 3719 Pa over a scaffold length of 10mm, resulting in a gradient slope of 341±23.9 Pa/mm (R^2 = 0.84) while the immobilized RGD concentration remained uniform at 3.53±0.28 mM (Figure 4A). In addition, modulus gradient hydrogels exhibited spatial variations in proteolytic degradation rate, which is

expected as the crosslinker was modified to contain protease-sensitive peptide sequences. The bottom-most section of the scaffold (2mm) exhibiting the lowest elastic modulus degraded most rapidly while the upper-most section, associated with the highest elastic modulus (10mm), exhibited the longest degradation time (Figure 4B). For elastic modulus gradient hydrogels the time for complete material degradation increased linearly from 24 hrs to 56 hrs along the imposed gradients (Figure 4C). In brief, creation of hydrogel scaffolds with gradients in elastic modulus and decoupled variations in immobilized RGD were successfully created. It must be noted that variations in proteolytic degradation rate are inherently coupled to modulus and inversely correlated with increases in elastic modulus using this chemistry.

In the case of modulus gradient hydrogel scaffolds, acquired confocal images of vascular sprouts emanating from spheroids and quantification of sprout length by angle are shown in Figure 4 D–L. Relatively uniform sprouting was observed in spheroids embedded within all three regions of elastic modulus gradient scaffolds at days 7 and 14. Minimal increases in spatial variations in vascular sprouting were observed from day 7 to day 14. Comparisons of regional sprouting responses at a particular time point revealed increased sprouting in regions associated with low compared to high elastic modulus. In covalently crosslinked PEG-based hydrogels variations in mechanical properties (due to changes in crosslinker composition) correlate with alterations in network characteristics, including mesh size that may impact nutrient transport and diffusion in 3D culture. VEGF-165 is a critical mediator of neovascularization and exhibits the highest molecular weight (45 kDa) among the growth factor components in the culture media used in vitro studies. To determine if the observed vascular sprouting responses were due to differences in nutrient diffusion within the elastic modulus gradient scaffolds, the diffusion coefficient of VEGF-165 of the different gel sections (top, middle and bottom) was estimated using the free-volume approach proposed by Lustig and Peppas[31] which describes drug diffusivity and gel mesh size from swelling experiments. In gels possessing gradients of elastic modulus, mean hydrogel mesh size estimated using the Flory-Rehner equation[32] described in supporting information ranged from 127.04±3.31 nm, 122.88±3.01 nm, to 98.15±15.70 nm while the VEGF diffusion coefficient in the gel remained fairly uniform from $9.99\times10^{-7}\pm 9.99\times10^{-10}$ cm^2/sec, $9.98\times10^{-7}\pm9.40\times10^{-10}$ cm^2/sec to $9.99\times10^{-7}\pm 8.47\times10^{-9}$ cm^2/sec in regions of low modulus to high modulus, respectively. These results suggest that no significant variations in VEGF and/or nutrient diffusivity along the elastic modulus gradient that would differentially impact the observed cell responses.

2.3 Gradients in protease-sensitivity lead to spatial variations in scaffold degradation rate and vascular sprouting

Controlled rates of proteolytic degradation are critical to vascularized tissue remodeling as scaffolds exhibiting degradation rates that either exceed or significantly lag rates of matrix remodeling impede tissue regeneration. Importantly, a variety of complex, heterogeneous tissues exhibit spatial variations in proteolytic degradation and remodeling rates *in vivo*.[16,33] Thus, engineering scaffolds with gradients in protease-sensitivity is necessary for understanding their influence on vascularized tissue remodeling. Scaffolds exhibiting gradients in proteolytic sensitivity/degradation were created by gradually increasing the

molar ratio of DSite PEGDA to SSite PEGDA while keeping the total concentration of PEGDA and RGD-PEGMA concentration constant in the precursor solution fed into reaction vessel over time. In scaffolds containing gradients in proteolytic degradation, the immobilized RGD concentration and initial (prior to material degradation) elastic modulus remained uniform at 3.49±0.39mM and 2036±209 Pa, respectively (Figure 5A). Imposed spatial variations in degradation kinetics were due to differences in MMP-sensitivity exhibited between SSite and DSite peptide containing macromers. The bottom region of the scaffolds (2mm) crosslinked with highest molar ratio of SSite PEGDA exhibited the slowest degradation while the uppermost (10mm) section crosslinked with highest molar ratio of DSite PEGDA exhibited the most rapid degradation (Figure 5B). As shown in Figure 5C, the time required for complete hydrogel degradation ranged from 48 hrs to 8 hrs along the gradient and decreased with increasing distance from the initiation region of the ascending hydrogel front (bottom hydrogel region). In summary, our approach allowed us to create hydrogel scaffolds with gradients in proteolytic degradation without inducing regional variations in immobilized RGD concentration and initial elastic modulus.

Similar to the findings observed in modulus gradient hydrogels, spheroids embedded in hydrogel scaffolds exhibiting spatial variations in protease-sensitivity exhibited unbiased sprouting in all three regions at days 7 and 14 (Figure 5 D–L). Spatial variations in vascular sprouting responses were observed in these gradient scaffolds with regions exhibiting the highest protease-sensitivity or fastest degradation (top region) inducing maximal sprouting in comparison to the slower degrading regions.

2.4 Combined gradient scaffolds influence overall and biased vascular sprouting responses

A variety of complex tissues possess opposing or concurrent gradients in matrix cues. To understand the impact of these gradient characteristics on vascular sprouting responses we created gradient hydrogel scaffolds with concurrent gradients in immobilized RGD and protease sensitivity and an opposing gradient in elastic modulus. This was achieved by simultaneously increasing the molar ratio of RGD-PEGMA to PEGMA and the molar ratio of DSite PEGDA to SSite PEGDA, decreasing the total concentration of PEGDA and maintaining a constant macromer concentration of PEG monoacrylates in the precursor solution fed into reaction vessel over time. Using this approach, scaffolds presenting an increasing gradient in immobilized RGD concentration (0.76–3.40 mM; gradient slope of 321±22 μM/mm, R^2 = 0.94) and a decreasing gradient of elastic modulus (3782–1153 Pa; gradient slope of 338±26 Pa/mm, R^2 = 0.93) were created (Figure 6A). These combined gradient scaffolds were also designed to exhibit spatial variations in proteolytic degradation rate. The bottom (2mm) scaffold regions associated with a high elastic modulus and crosslinked with the highest concentration of SSite PEGDA exhibited the slowest degradation while the upper (10mm) region possessing a low elastic modulus that was crosslinked with highest concentration of DSite PEGDA exhibited the most rapid degradation (Figure 6B). It must be noted that polymerization of these two types of protease-sensitive crosslinkers allows for preservation of the imposed initial (prior to degradation) RGD and modulus gradients. As demonstrated in Figure 6C, the time required for complete degradation ranged from 52 hrs to 4 hrs across the entire hydrogel and decreased spatially

along the imposed gradient(s). In these combined gradient scaffolds, spatial variations in both overall and biased sprouting responses were observed (Figure 6D–L). Overall sprout outgrowth increased with increases in immobilized RGD concentration and protease-sensitivity and with decreases in elastic modulus. As a result, maximal sprout formation was observed in the top scaffold region (exhibiting the highest immobilized RGD concentration and protease-sensitivity and lowest elastic modulus) at both days 7 and 14. In addition, spheroids embedded in this region of the gradient scaffold exhibited biased sprouting at 45°,0°and 45°with gradient.

2.5 Quantitative analysis of vascular sprouting responses in gradient scaffolds

As each gradient hydrogel scaffold induces spatial variations in overall cumulative sprout length, the cumulative sprout length of spheroids in all three regions of all five gradient hydrogel scaffolds was quantified (Figure 7a). At day 7, all gradient scaffolds, except for those exhibiting shallow gradients in immobilized RGD, induced significant spatial variations in cumulative sprout length (Figure 7A). Three-dimensional volume renderings of spheroids within steep RGD gradient hydrogels also demonstrated the observed differences in spatial variations in vascular sprouting (Figure 7D–F and Supplemental Video). Among all gradient scaffolds, the combined gradient hydrogel scaffolds induced the highest sprout length (36,000 μm) which was found to be 60-fold higher in regions containing the highest immobilized RGD concentration and protease-sensitivity and lowest elastic modulus compared to low RGD and protease-sensitivity and high modulus regions. At day 14, all gradient hydrogel scaffolds exhibited significant spatial variations in cumulative sprout length in similar patterns as those found at day 7 (Figure 7B). However, the fold increase in cumulative sprout length from day 7 to day 14 was generally found to be between 1.5 to 2. It is worth noting that spheroids in the middle region of steep RGD gradient hydrogels as well as top and bottom regions of shallow RGD gradient hydrogels exhibited a 5–7 fold increase in cumulative sprout length.

As vascular spheroids exhibited various degrees of biased sprout formation in response to different types of gradients, the gradient bias index was calculated as a measure of the “attractiveness of the gradients on vascular sprouting. Figure 8 summarizes the gradient bias index with 95% confidence intervals as error bars, and the gradient bias index is considered significantly higher or lower than 0 if the 95% confidence interval does not include 0. At day 7, significant biased sprouting of spheroids is observed in steep RGD gradient (top, middle and bottom), shallow RGD gradient (top and middle), modulus gradient (top and middle) and combined gradient (top) hydrogel scaffolds. It worth noting that the gradient bias index in the case of modulus gradient scaffolds was found to be negative indicating that the modulus gradient exerted a “repulsive” as opposed to an “attractive” effect on vascular sprouting. Similar trends were observed by day 14; however, biased sprouting responses were no longer significant at this time point. In addition, spheroids encapsulated in bottom regions of shallow RGD gradient hydrogels and middle regions of the combined gradient hydrogel also exhibited significant biased sprouting. Spatial variations of gradient bias index were observed in both steep and shallow RGD gradient scaffolds. Spheroids encapsulated in the top and middle regions of both steep and shallow RGD gradient hydrogel scaffolds exhibited significantly higher sprouting compared to those in bottom regions of the

respective gradient scaffolds. These findings suggest that the effect of the RGD gradient on vascular sprouting is dependent on the magnitude of the local RGD concentration. It is worth noting that the middle region of the steep RGD gradient hydrogel scaffolds and the top region of the shallow RGD gradient hydrogel scaffolds present a similar RGD concentration (1.7mM and1.9mM, respectively) but a different gradient slope (322±31 μM/mm and 160±15 μM/mm, respectively). Spheroids encapsulated in the middle region of the steep RGD gradient hydrogel scaffolds exhibited a significantly higher gradient bias index in comparison to those in top region of the shallow RGD gradient hydrogel scaffolds. This suggests that the slope of the RGD gradient also independently influences the preferential growth of vascular sprouts. Spheroids encapsulated in elastic modulus and/or protease-sensitivity gradient hydrogel scaffolds did not exhibit significant spatial variations in gradient bias index which suggests that the magnitude of local matrix properties has minimal or no effect on gradient preferential growth of vascular sprouts. Lastly, the gradient bias indexes of spheroids in the combined gradient hydrogel were lower than those observed in steep and shallow RGD gradient hydrogels even though both scaffolds present the same immobilized RGD concentration gradient. This suggests that the effects of RGD gradients on biased sprouting could be influenced by spatial variations in other matrix properties.

3 Discussion

Vascularization of complex tissues including those exhibiting spatial heterogeneity in extracellular matrix biochemical composition and mechanical properties remains as a major obstacle in tissue engineering.[1–3] Understanding how the process of neovascularization is influenced by spatial variations of biochemical and biomechanical signals provided by an engineered scaffold is crucial when designing biomaterials that promote vascularization and complex tissue formation simultaneously. In addition, scaffolds presenting gradients in immobilized biosignaling molecules may enhance vascularized tissue formation as the native process of neovascularization is regulated by spatiotemporal ECM cues.[3]Biomaterial platforms that incorporate spatiotemporal variations in immobilized biochemical composition, mechanical and structural properties, however, have been challenging to develop and thus the role of these gradients on engineering vascularized tissues is not well understood. Here, we used a gradient hydrogel fabrication method to create cell-laden hydrogel scaffolds with robust and decoupled gradients of cell adhesion ligands, elastic modulus and protease-sensitivity to study their impact on vascular cell responses in 3D culture. To our knowledge, this is the first study to investigate neovascularization responses to spatial variations in these cues within cell-laden gradient hydrogel scaffolds.

Due to the versatility of our gradient scaffold generation platform, a variety of signals could be spatially embedded within hydrogel scaffolds. As a proof-of-concept, by design we selected to generate (1) gradients in RGD concentration, since cell adhesive integrin binding peptides represent the minimal and ubiquitous biochemical signal present in ECM tissues required for cell adhesion and survival,[34] (2) gradients in elastic modulus, as mechanical stiffness gradients exist in a variety of heterogeneous and complex interfacial tissues including those involving bone and cartilage interfaces,[16,35] and (3) gradients in protease-sensitivity, since tuning of proteolytic scaffold degradation can be tailored to specific cell types and variable tissue remodeling rates which exist natively in complex heterogeneous

tissues.[36] The magnitude of each of these gradients was selected based on our recently published study focused on an experimental sensitivity and statistical design of experiment (DOE) analysis that identified optimal ranges of these matrix cues which supported vascular sprouting within isotropic scaffolds in 3D culture.[30] Hydrogel scaffolds with spatial variations of immobilized RGD concentration, elastic modulus and proteolytic degradation rate were generated and carefully characterized to ensure each gradient was created without imposing changes in other hydrogel properties (Figure 6). While most gradient material fabrication methods enable generation of a single type of gradient,[37–40] our method is capable of creating scaffolds with multiple types of gradients, as well as combining concurrent and opposing gradients in single scaffold without affecting the characteristics of other imposed gradients. These inherent features allowed us to investigate the individual and synergistic effects of gradient properties on vascular sprouting responses in 3D culture.

By encapsulating individual vascular spheroids in different regions along the gradient within the scaffold (top, middle and bottom), we evaluated the impact of the imposed gradients on spatial variations in total cumulative sprout length (CSL) as well as directional sprouting. In addition, we also investigated whether the presence of the gradient(s) induced guided neovascularization by measuring the gradient bias index in response to gradient type, slope and magnitude. Total CSLs varied significantly among spatial regions within each gradient scaffold and generally increased with increases in immobilized RGD concentration, decreases in elastic modulus and increases in protease-sensitivity (Figure 7). Spatial variations in the extent of vascular sprouting within scaffolds might be desired for engineering of complex tissues such as osteochondral tissues in which bone regeneration requires the presence of a dense vascular network, while the cartilage region is avascular. In addition, successful regeneration of these tissues requires the presence of linear and continuous gradients in scaffold mechanical properties, biochemical composition and material degradation time as the remodeling rates of these tissues significantly differ.[16] However, restoration of other interfacial tissues such as bone-to-tendon or bone-to-ligament interface tissues would require vascularization of the entire scaffold. In these tissues a mechanical stiffness gradient might be embedded in the scaffold to induce spatial differentiation and protein expression.[35] The findings of our study suggest that modulus gradients lead to spatial variations in 3D neovascularization with stiffer regions inhibiting vascular invasion. Based on the findings of vascular sprouting, the addition of a protease-sensitivity gradient has potential to counter the observed cellular effect induced by gradients in modulus. Nevertheless, vascularization of complex tissues possessing gradients in matrix properties requires careful scaffold design criteria to achieve optimal outcomes.

Another notable result in our study is the observed biased vascular sprouting responses in RGD gradient scaffolds with steep and shallow slopes and in the combined gradient scaffolds (Figure 3 and 6). Studies in the literature have shown that gradients in cell adhesion, including fibronectin, collagen, laminin and adhesive peptide ligands of RGD, guide migration or alignment of various vascular cells, including endothelial cells, fibroblasts and smooth muscle cells.[21,24,41,42] The vascular sprouts in our study appear to grow under spatial guidance of immobilized RGD concentration gradients. Since vascular sprouts are led by tip cells (specialized endothelial cells associated with a migratory phenotype) we hypothesize that the observed preferential sprouting responses could be the

result of directional tip cell migration, however, further studies are required to confirm the observed phenotype. Furthermore, the extent of preferential growth of sprouts toward the imposed gradient (i.e. gradient bias index) decreased significantly as the RGD concentration magnitude decreased in different hydrogel regions. This suggests that the local RGD concentration plays a significant role on guiding vascular sprouting and higher RGD concentration promotes more extensive directional sprout formation. When comparing the gradient bias index of spheroids exposed to the same RGD magnitude but different gradient slope, we found that the slope of RGD gradient also independently influenced directional sprouting. Our findings also suggest that immobilized RGD concentration gradients induce biased directional vascular sprout formation in the increasing RGD concentration direction. Furthermore, this response appears to increase with immobilized RGD concentration magnitude and gradient slope. Interestingly, previous studies involving 2D cell migration of endothelial and fibroblast cells in response to gradients of immobilized RGD have similarly observed that migration is influenced by both gradient and magnitude of RGD concentration.[24]Although variations in the slope of MMP-sensitivity and the elastic modulus gradients may also influence regional vascular sprouting behavior, this response would also be influenced by local uniform peptide concentration(, immobilized RGD and MMP-sensitivity) and matrix properties (modulus and degradation rate). Since native tissue remodeling rates and modulus vary over a broad range of different tissue types the impact of gradients in proteolytic degradation and mechanical properties on vascularization will be explored in future studies which focus on regeneration of more complex tissues includingthose involving interfacial osteochondral tissues which natively exhibit gradients in elastic modulus, rates of proteolytic remodeling and regional vascularization.

After observing the effects of each gradient type on 3D vascular sprouting, we hypothesized that presenting all three gradients in a manner that induces the most (high RGD concentration, low elastic modulus and high protease-sensitivity) and least (low RGD concentration, high elastic modulus and low protease-sensitivity) favorable conditions for sprouting to vascular spheroids would synergistically enhance biased sprouting responses originally observed in RGD gradient hydrogels. Our findings demonstrated that spheroids encapsulated in regions with the most preferable properties exhibited significant enhancements in total CSL compared to those in the bottom regions. However, the combined gradient did not enhance biasing as hypothesized. Instead, combined gradient scaffolds resulted in a lower biased index in vascular sprouting compared that observed in steep RGD gradient scaffolds. Whether the modulus gradient, the protease-sensitivity gradient, or the combination of three gradients contributed to the observed phenomena s is unclear and warrants further investigation. We speculate that the guidance cues provided by the RGD gradient may be modulus dependent since the steep RGD gradient hydrogel contained a uniform but high elastic modulus (4 kPa) while regions exhibiting the highest RGD concentration in the combined gradient scaffold possessed a lower modulus (1.2 kPa). Although high modulus was found to inhibit overall sprouting, it may be required in the case were induced biased sprouting in response to RGD gradients is desired. One limitation of our current study is that vascular sprouting responses were evaluated using static images at distinct time points (i.e. days 7 and 14) rather than by tracking the cells dynamically. Future

studies will focus on the use of GFP-transfected cells evaluate vascular sprouting morphology changes in response to embedded matrix gradient matrix properties.

4 Conclusion

In this study we designed vascular cell-laden gradient PEG hydrogels with 5 types of gradient combinations in immobilized RGD, stiffness and protease-sensitivity and explored the impact of these gradients on spatial variations in supporting vascular sprouting within the constructs in 3D culture. Regional encapsulation of co-culture spheroids along the imposed gradient(s) in scaffolds led to spatial variations in total sprout length. In addition, we found that RGD gradient and combined gradient scaffolds promoted biased sprouting toward increasing RGD concentration which was found to be dependent on RGD gradient magnitude and slope. Conversely, biasing in vascular sprouting was diminished in the combined gradient scaffolds. The presented work is the first to demonstrate the implementation of a cell-laden hydrogel scaffold to explore the impact of gradients in RGD, proteolytic degradation and stiffness on vascular sprouting responses in 3D culture. The presented platform and findings of this work hold great potential for pre-vascularization of complex tissues and for inducing spatial variations of vascularization of complex tissues that require gradients in mechanical properties, degradation rate and adhesion ligand composition for their regeneration.

5 Experimental Section

5.1 Materials

Dimethylformamide (DMF), O-benzotriazole-N,N,N,N-tetra-methyl-uronium-hexafluoro-phosphate (HBTU), tri- fluoroacetic acid (TFA), Fmoc-amino acids, and the Wang resin were obtained from AAPPTec (Louisville, KY). N,N-Diisopropylethyl- amine (DIEA), thioanisole, triisopropylsilane (TIS), and diethyl ether were obtained from Fisher Scientific (Hanover Park, IL). Piperidine, phenol, N-vinylpyrrolidone (NVP), tri-ethanolamine (TEA), and eosin Y were obtained from Sigma-Aldrich (St. Louis, MO).

5.2 Peptide Synthesis, Design, and Purification

Scaffolds were rendered susceptible to cell-mediated proteolysis by incorporating MMP-sensitive peptide sequences VPMS↓MR (↓ denotes cleavage point) within network crosslinks. To control scaffold degradation without inducing variations in scaffold modulus, MMP-sensitive peptides containing one and two repeats of the VPMSMR sequence (GG**VPMS↓MR**GGK or SSite) and (GG**VPMS↓MR**GDG**VPMS↓MR**GGK or DSite) were synthesized using solid phase peptide synthesis and conjugated to Acrylate-PEG-SVA heterobifunctional macromers to create crosslinkers of similar molecular weight but varying protease-sensitivity as described below. The YRGDS peptide sequence was also synthesized and conjugated to Acryl-PEG-SVA leading to its immobilization into the hydrogel matrix following polymerization to enable cell adhesion. All peptides were synthesized using solid-phase peptide synthesis based on standard Fmoc chemistry on a Focus Xi automated peptide synthesizer (AAPPTec, Louisville, KY). Amino acid coupling was carried out on a Wang resin in the presence of DIEA and HBTU. The Fmoc group was deprotected with 20%

piperidine in DMF. Peptides were cleaved from the resin and deprotected in a TFA cleavage cocktail (90% TFA, 2.5% TIS, 2.5% thioanisole, 2.5% (w/v) phenol, and 2.5% deionized water) for 2.5 h, precipitated in cold diethyl ether, and purified by reverse-phase high-performance liquid chromatography (HPLC). Peptide purity was confirmed by ion trap time-of-flight (IT-TOF) mass spectroscopy. Purified peptides were lyophilized and stored at −20°C until use.

5.3 Synthesis of Difunctional and Monofunctional Photopolymerizable PEG Macromers

Four types of photopolymerizable macromers were synthesized and used to create cell-adhesive and proteolytically degradable hydrogel scaffolds with tunable variations in immobilized RGD concentration, elastic modulus and protease-sensitivity. These included, poly(ethylene) glycol (PEG) diacrylate (PEGDA) cross-linkers of similar molecular weight containing (1) one (SSite) or (2) two (DSite) MMP-sensitive peptide cleavage sites between terminal acrylate groups of the PEGDA crosslinker, (3) an RGD-containing PEG monoacrylate macromer (RGD-PEGMA) and (4) a PEG monoacrylate macromer (PEGMA) of molecular weight similar to RGD-PEGMA used as a surrogate during polymerization used to modulate RGD concentration without inducing variations in scaffold degradation or modulus. SSite and DSite PEGDA crosslinkers were synthesized via conjugation of SSite and DSite MMP-sensitive peptides to Acryl-PEG_{5000}-SVA (Laysan Bio, Arab, AL, MW= 5 kDa) in a 2:1 PEG to peptide molar ratio yielding Acryl-PEG_{5000}- GGVPMS↓MRGGK-PEG_{5000}-Acryl (MW≈ 11 kDa) and Acryl-PEG_{5000}- GGVPMS↓MRGDGVP PEG_{5000}-Acryl (MW ≈ 12 kDa), respectively. The cell- adhesive peptide YRGDS was conjugated to Acrylate-PEG_{3400}-SVA in a 1:1 PEG to peptide molar ratio, to yield the photopolymerizable RGD-PEGMA monofunctional macromer, Acryl-PEG_{3400}-YRGDS (MW ≈ 4 kDa). A tyrosine residue (Y) was added to the peptide sequence to quantify the immobilized RGD concentration in the scaffold by radiolabeling the tyrosine with ^{125}I (described below). Peptide conjugation reactions were carried out in $NaHCO_3$ solution (50mM, pH 8.0) for 4 h while protected from light. The conjugated solution was dialyzed for 24 h to removed unreacted reagents, lyophilized, and stored at −20 °C until use. PEGMA (MW = 5kDa) was synthesized through acrylation of monomethoxy-PEG_{5000} (MW = 5 kDa) using a two-fold molar excess of acryloyl chloride relative to free hydroxyls in the presence of trimethylamine in anhydrous dichloromethane under argon overnight in the dark. The resulting product was separated from aqueous byproducts by the addition of K_2CO_3 (2M). The organic phase was collected in a separatory funnel and the final PEGMA solution was precipitated in ice-cold ether, filtered, dried under vacuum overnight, and stored at 20 °C until use. Acrylation efficiency of PEGMA was confirmed to be > 95% using 1H NMR.

5.4 Fabrication of Cell-Laden Gradient Hydrogel Scaffolds

Ascending frontal photopolymerization[28] was used to create five distinct cell-laden gradient hydrogels using two programmable syringe pumps to deliver distinct precursor solutions into a transparent reaction chamber (5 mm 10 mm 20 mm) which was exposed to a visible light (λ = 514 nm) using an argon ion laser (Coherent, Santa Clara, CA) at a laser flux of 100 mW/cm^2. Hydrogel crosslinking occurred continuously with the ascending reaction front as precursor solutions were fed to the reaction vessel. Whereas the syringe pumps were programmed to deliver precursor for 5 min, the photopolymerization was carried out for a

total of 10 min to ensure that every region of the precursor was photopolymerized for at least 5 min. The scaffolds presented (1) steep and (2) shallow gradients in RGD with uniform modulus and protease-sensitivity, (3) gradients in elastic modulus with uniform RGD concentration and protease-sensitivity, (4) gradients in protease-sensitivity with uniform RGD concentration and modulus, and (5) a concurrent RGD and protease-sensitivity gradient and a countercurrent or opposing modulus gradient. Gradients in RGD concentration, elastic modulus and protease-sensitivity were induced by spatial distribution of the macromer composition in the precursor feed (Figure1). To create hydrogels with a steep gradient in immobilized RGD concentration, the gradient profile was designed with an increasing and decreasing concentration of RGD-PEGMA (0–5 mM) and PEGMA (5 to 0 mM), respectively while maintaining a constant DSite PEGDA precursor concentration (2.5mM) during polymerization. To create hydrogels with shallow gradients in immobilized RGD, the gradient profile was designed with increasing and decreasing concentrations of RGD-PEGMA (0 to 2.5 mM) and PEGMA (5 to 2.5 mM), respectively while maintaining a constant DSite PEGDA precursor concentration (2.5mM) during polymerization. Fabrication of elastic modulus gradient hydrogels was achieved by increasing the SSite PEGDA precursor concentration (1.5 to 2.5 mM) while maintaining a constant precursor concentration of RGD-PEGMA (5mM). To induce gradients in protease-sensitivity within scaffolds, one syringe pump was programmed to supply a precursor feed with an increasing concentration of DSite PEGDA (0 to 2 mM) while the second pump provided a decreasing concentration of SSite PEGDA (2 to 0 mM) while maintaining the RGD-PEGMA concentration (5mM) constant during photopolymerization. Finally, hydrogels with concurrent gradients in RGD and protease-sensitivity and an opposing elastic modulus gradient were created through simultaneous increases in RGD-PEGMA (0 to 5 mM), decreases in PEGMA (5 to 0 mM), increases in DSite PEGDA (0 to 1.5 mM) and decreases in SSite PEGDA (2.5 to 0mM) precursor feed concentrations during crosslinking. The precursor conditions used to create the different types of gradient scaffolds are summarized in Figure 1. All precursor solutions consisted of NVP (accelerator and comonomer, 37 mM), TEA (co-initiator, 7 mM), and eosin Y (photoinitiator, 0.05 mM) using phosphate buffer solution (PBS),pH 7.4, as the solvent. Following photopolymerization, gradient hydrogels were removed from the reaction vessel, soaked in PBS or DI water for 48 h to allow for equilibrium swelling and sectioned into seven 2 mm thick segments along the gradient using an array of razor blades. The first and last sections were discarded (to avoid characterization of edge effects) and the remaining five sections used to quantify variation in immobilized RGD concentration, elastic modulus and degradation kinetics. Each hydrogel section is designated based on a distance from which the ascending hydrogel front was initiated the notations y=2mm, 4mm, 6mm, 8mm and 10mm represent the distances along the imposed gradient(s)(y-direction) from the initial region of ascending hydrogel front (Figure 2). To evaluate spatiotemporal effects of scaffold properties on 3D neovascularization a co-culture spheroid assay of sprouting angiogenesis recapitulating the multicellular and coordinated process of neovascularization[43] was utilized. Cell spheroids composed of 50% human umbilical vascular endothelial cells (HUVECs, Lonza) and 50% human umbilical arterial smooth muscle cells (HUASMCs, Lonza) were formed by suspending both cells types (5000 total cells/well) in culture media containing 0.24% (w/v) methyl cellulose in round-bottomed, low binding, 96-well plates and incubated overnight at 37 °C and 5% CO_2. Prior

to hydrogel fabrication, individual spheroids along with 1μL of culture media were pipetted into a glass capillary tube (ID 1 mm) and separated by a small segment of air which prevented spheroid aggregation (Figure 2). Using a syringe pump and a 100μL Hamilton syringe, spheroids were added into the reaction chamber along with the precursor solution and photoencapsulated within gradient hydrogels upon polymerization. The delivery of spheroids was scheduled so that at least three spheroids were spatially photoencapsulated within scaffolds along the gradient(s) (y-direction, Figure 2). Specifically, spheroids were regionally positioned in (1) in the bottom (y=1–3mm), (2) middle (y=4–6mm) and (3) top (y=7–9mm) region of gradient hydrogels. A representative image of regional spheroid encapsulation in gradient scaffolds is shown in Figure S2.

5.5 Quantification of Immobilized RGD Concentration

The incorporation of immobilized YRGDS was quantified by tracking the radioactivity of radiolabeled (with ^{125}I) tyrosine residues (Y) prior to gel formation and subsequent to hydrogel formation as described in our previous studies. (Turturro2013b,He2018a) Briefly, 5 mg of YRGDS was dissolved in reaction buffer (1 PBS, pH 6.5), combined with 1mCi sodium iodine (PerkinElmer Health Sciences) in the presence of iodination beads (Pierce)and allowed to react for 15 min. Radiolabeled RGD (^{125}I-YRGDS) was conjugated to Acryl- PEG_{3400}-SVA as described above) to generate a radiolabeled RGD-PEGMA macromer. To track the spatial incorporation of the YRGDS adhesion ligand in gradient scaffolds, radiolabeled Acryl-PEG_{3400}-YRGDS was added to the precursor in an amount not exceeding 20 wt % of the total peptide. Hydrogel sections were swollen in DI water for 48 h with three water changes and hydrogel radioactivity measured using a Multi-Wiper gamma counter (Laboratory, Technologies, Inc. Elburn, IL). Hydrogels were subsequently weighed in the fully-swollen state, frozen at −80 °C, lyophilized and the dry weight recorded. The immobilized RGD concentration in the hydrogel, $[RGD]_{gel}$, was calculated according to following the equation:

$$[RGD]_{gel} = \frac{R \times SA}{\frac{m_{swollen} - m_{dried}}{\rho_{water}} + \frac{m_{dried}}{\rho_{PEG}}} \quad (1)$$

where R is the measured radioactivity, SA is the specific activity (mole/Ci) that was measured and used to convert the measured radioactivity to moles of peptide, $m_{swollen}$ is the equilibrium the swollen weight of the hydrogel, m_{dried} is the weight of the hydrogel in the dried state, ρ_{water} is density of water at room temperature (0.997 g/ml) and ρ_{PEG} is the density of PEG (MW=10 kDa) at room temperature (1.3 g/ml).

5.6 Quantification of Elastic Modulus

Spatial variations in elastic modulus were quantified using uniaxial compression experiments. Hydrogel sections were loaded onto a Chatillon TCD200 mechanical tester (Wagner Instruments). Samples were compressed at a rate of 0.5 mm/min, and the elastic modulus of each section was quantified from the slope of the linear region (< 10% strain, r^2 > 0.95) of the stressstrain curve.

5.7 Quantification of Hydrogel Degradation Kinetics

The degradation profiles of fully swollen protease-sensitive PEGDA scaffolds were obtained gravimetrically by incubation with interstitial collagenase (Collagenase-IA from Clostridium histolyticum, SigmaAldrich) enzyme solution in 10 mM HBS with 1 mM $CaCl_2$ (pH 7.4) at a concentration of 0.1 μg/mL at 37 °C. Swollen weight of hydrogels was recorded at pre-determined time points the after which fresh enzyme solution was replenished at every time point until complete hydrogel degradation was achieved.

5.8 Evaluation of 3D Vascular Sprouting Response to Scaffold Embedded Gradients

Spheroid-laden gradient hydrogels were rotated and laid flat on their side in a 6-well plate, and were cultured in endothelial cell growth medium (EGM, Cell Applications, Inc.) with media changes every other day. At days 7 and 14, hydrogel scaffolds were fixed with 4% paraformaldehyde and stained for F-actin with Alexa Fluor 546-phalloidin (25U/ml) and fluorescein labeled Ulex Europaeus Agglutinin I (UEA I), a marker for human endothelial cells. Stained spheroids were imaged using PASCAL laser scanning confocal microscopy (Carl Zeiss MicroImaging, Inc.) with a 5× objective to produce a series of z-stack images at 10 μm intervals that were used to generate 3D volume rendering using volume Viewer command in MATLAB or flattened to obtain maximum intensity z-projected images. Final images were analyzed with sprout ImageJ/Fiji to produce measurements of maximum sprout length along eight different directions where the 0°and 180°represent the directions along the gradient including the top (y=10mm) and bottom regions of the hydrogel (y=0mm), respectively. In addition, we used the morphology plugin of ImageJ/Fiji to quantify cumulative sprout length (CSL) of the entire image as well as the upper segment (−45°to +45°) and lower segment (−135°to +135°). These measurements were used to calculate a gradient bias index of vascular sprouting using the following equation:

$$\text{Gradient Bias Index} = \frac{CSL_{-45^\circ to +45^\circ} - CSL_{-135^\circ to +135^\circ}}{CSL_{total}} \quad (2)$$

In equation (2), $CSL_{-45^\circ to +45^\circ}$ and $CSL_{-135^\circ to +135^\circ}$ denote the cumulative sprout length measured within the top segment (−45°to +45°) and bottom (−135°to +135°) gradient scaffold segments, respectively, and CSL_{total} denotes the cumulative sprout length of the entire spheroid.

5.9 Statistical Analysis

Three hydrogels (n=3) were fabricated to quantify spatial variations in immobilized RGD concentration, elastic modulus and degradation kinetics for each gradient scaffold group. To evaluate 3D vascular sprouting responses, three hydrogels (n=3) were fabricated for each gradient scaffold group within which 9–12 spheroids total were encapsulated in each hydrogel with 3–4 spheroids encapsulated in the top, middle and bottom regions of the gradient scaffold (Figure 2). Cumulative sprout length and gradient bias index were calculated for each encapsulated spheroid in each of the three gel regions and vascular sprouting parameters were averaged for each region across all hydrogels for a particular hydrogel group. All data are presented as mean±standard deviation or mean±95%

confidence intervals. To determine statistical significance between groups, one-way ANOVA as well as two-way ANOVA was performed followed by a Tukeys HSD post-test for pairwise and multiple group comparisons (GraphPad Prisim8). In all cases, p-values < 0.05 were considered statistically significant.

Supplementary Material

Refer to Web version on PubMed Central for supplementary material.

Acknowledgements

We thank Dr. Joseph Orgel and Dr. Rama Sashank Madhurapantula of the College of Science and Letters at the Illinois Institute of Technologyfor for access to HPLC and assistance with peptide purification. We also thank Cecilie Tassone of PraxiCut Inc for the access of mechanical tester at mHub. This research was supported by funding from the National Institutes of Health Grant (R21AR074072–01A1) awarded to G.P. (PI) and the National Science Foundation REU Grant (NSF grant EEC 1461215) awarded to J.G..

References

1. Levenberg S, Rouwkema J, Macdonald M, Garfein ES, Kohane DS, Darland DC, Marini R, Van Blitterswijk CA, Mulligan RC, D'Amore PA, Langer R, Nature Biotechnology 2005, 23, 7 879.
2. Lamalice L, Le Boeuf F, Huot J, Circulation Research 2007, 100, 6 782. [PubMed: 17395884]
3. Turturro M, Papavasiliou G, In Vascularization, 312, chapter 9, 163–190, ISBN 978–1-4665–8046-6, 2014, URL http://www.crcnetbase.com/doi/abs/10.1201/b16777-12.
4. Moon JJ, Saik JE, Poché RA, Leslie-Barbick JE, Lee SH, Smith AA, Dickinson ME, West JL, Biomaterials 2010, 31, 14 3840. [PubMed: 20185173]
5. Vigen M, Ceccarelli J, Putnam AJ, Macromolecular Bioscience 2014, 14, 10 1368. [PubMed: 24943402]
6. Pike DB, Cai S, Pomraning KR, Firpo MA, Fisher RJ, Zheng X, Prestwich GD, Peattie RA, Shu XZ, Prestwich GD, Peattie RA, Biomaterials 2006, 27, 30 5242. [PubMed: 16806456]
7. Zieris A, Chwalek K, Prokoph S, Levental KR, Welzel PB, Freudenberg U, Werner C, Journal of controlled release : official journal of the Controlled Release Society 2011, 156, 1 28. [PubMed: 21978645]
8. Moulisová V, Gonzalez-García C, Cantini M, Rodrigo-Navarro A, Weaver J, Costell M, Sabater i Serra R, Dalby MJ, García AJ, Salmerón-Sánchez M, Biomaterials 2017, 126 61. [PubMed: 28279265]
9. Schweller RM, Wu ZJ, Klitzman B, West JL, Annals of Biomedical Engineering 2017, 45, 6 1387. [PubMed: 28361182]
10. Papavasiliou G, Cheng M-H, Brey EM, Journal of Investigative Medicine 2010, 58, 7 838. [PubMed: 20683343]
11. Koike N, Fukumura D, Gralla O, Au P, Schechner JS, Jain RK, Nature 2004, 428, 6979 138. [PubMed: 15014486]
12. Zhu W, Qu X, Zhu J, Ma X, Patel S, Liu J, Wang P, Lai CSE, Gou M, Xu Y, Zhang K, Chen S, Biomaterials 2017, 124, 2 106. [PubMed: 28192772]
13. Chen YC, Lin RZ, Qi H, Yang Y, Bae H, Melero-Martin JM, Khademhosseini A, Advanced Functional Materials 2012, 22, 10 2027. [PubMed: 22907987]
14. Sundararaghavan HG, Monteiro GA, Firestein BL, Shreiber DI, Biotechnology and Bioengineering 2009, 102, 2 632. [PubMed: 18767187]
15. Frantz C, Stewart KM, Weaver VM, Journal of Cell Science 2010, 123, 24 4195. [PubMed: 21123617]
16. Cross LM, Thakur A, Jalili NA, Detamore M, Gaharwar AK, Acta Biomaterialia 2016, 42 2. [PubMed: 27326917]
17. Cao L, Mooney DJ, Advanced Drug Delivery Reviews 2007, 59, 13 1340. [PubMed: 17868951]

18. Odedra D, Chiu LLY, Shoichet M, Radisic M, Acta Biomaterialia 2011, 7, 8 3027. [PubMed: 21601017]
19. Guo X, Elliott CG, Li Z, Xu Y, Hamilton DW, Guan J, Biomacromolecules 2012, 13, 10 3262. [PubMed: 22924876]
20. Akar B, Jiang B, Somo SI, Appel AA, Larson JC, Tichauer KM, Brey EM, Biomaterials 2015, 72 61. [PubMed: 26344364]
21. Smith JT, Tomfohr JK, Wells MC, Beebe TP, Kepler TB, Reichert WM, Langmuir : the ACS journal of surfaces and colloids 2004, 20, 19 8279. [PubMed: 15350103]
22. Liu L, Ratner BD, Sage EH, Jiang S, Langmuir 2007, 23, 22 11168. [PubMed: 17892312]
23. DeLong SA, Gobin AS, West JL, Journal of Controlled Release 2005, 109, 1–3 139. [PubMed: 16290119]
24. Guarnieri D, De Capua A, Ventre M, Borzacchiello A, Pedone C, Marasco D, Ruvo M, Netti P. a., Acta biomaterialia 2010, 6, 7 2532. [PubMed: 20051270]
25. Wong JY, Velasco A, Rajagopalan P, Pham Q, Langmuir 2003, 19, 5 1908.
26. Hadjipanayi E, Mudera V, Brown RA, Cell motility and the cytoskeleton 2009, 66, 3 121. [PubMed: 19170223]
27. Borselli C, Oliviero O, Battista S, Ambrosio L, Netti PA, Journal of Biomedical Materials Research Part A 2007, 80A, 2 297.
28. He YJ, Young DA, Mededovic M, Li K, Li C, Tichauer K, Venerus D, Papavasiliou G, Biomacromolecules 2018, 19, 11 4168. [PubMed: 30253093]
29. Jeon O, Alt DS, Linderman SW, Alsberg E, Advanced Materials 2013, 25, 44 6366. [PubMed: 23983019]
30. He YJ, Santana MF, Moucka M, Quirk J, Shuaibi A, Pimentel MB, Grossman S, Rashid MM, Cinar A, Georgiadis JG, Vaicik MK, Kawaji K, Venerus DC, Papavasiliou G, Journal of Biomaterials Science, Polymer Edition 2019, 0, 0 1.
31. Lin CC, Metters AT, Hydrogels in controlled release formulations: Network design and mathematical modeling, 2006.
32. Flory P, Principles of polymer chemistry, Cornell University Press, 1953.
33. Steinmetz NJ, Aisenbrey EA, Westbrook KK, Qi HJ, Bryant SJ, Acta Biomaterialia 2015, 21 142. [PubMed: 25900444]
34. Hern DL, Hubbell JA, J Biomed Mater Res 1998, 39, 2 266. [PubMed: 9457557]
35. Seidi A, Ramalingam M, Elloumi-Hannachi I, Ostrovidov S, Khademhosseini A, Acta Biomaterialia 2011, 7, 4 1441. [PubMed: 21232635]
36. Sokic S, Papavasiliou G, Tissue engineering. Part A 2012.
37. Campbell K, Groisman A, Lab Chip 2007, 7, 2 264. [PubMed: 17268630]
38. Burdick JA, Khademhosseini A, Langer R, Langmuir 2004, 20, 13 5153. [PubMed: 15986641]
39. Kloxin AM, Benton J. a., Anseth KS, Biomaterials 2010, 31, 1 1. [PubMed: 19788947]
40. Nemir S, Hayenga HN, West JL, Biotechnology and Bioengineering 2010, 105, 3 636. [PubMed: 19816965]
41. Cai K, Kong T, Wang L, Liu P, Yang W, Chen C, Colloids & Surfaces B: Biointerfaces 2010, 79, 1 291. [PubMed: 20462745]
42. Wu J, Mao Z, Gao C, Biomaterials 2012, 33, 3 810. [PubMed: 22048007]
43. Korff T, Kimmina S, Martiny-Baron G, Augustin HG, FASEB journal : official publication of the Federation of American Societies for Experimental Biology 2001, 15, 2 447. [PubMed: 11156960]

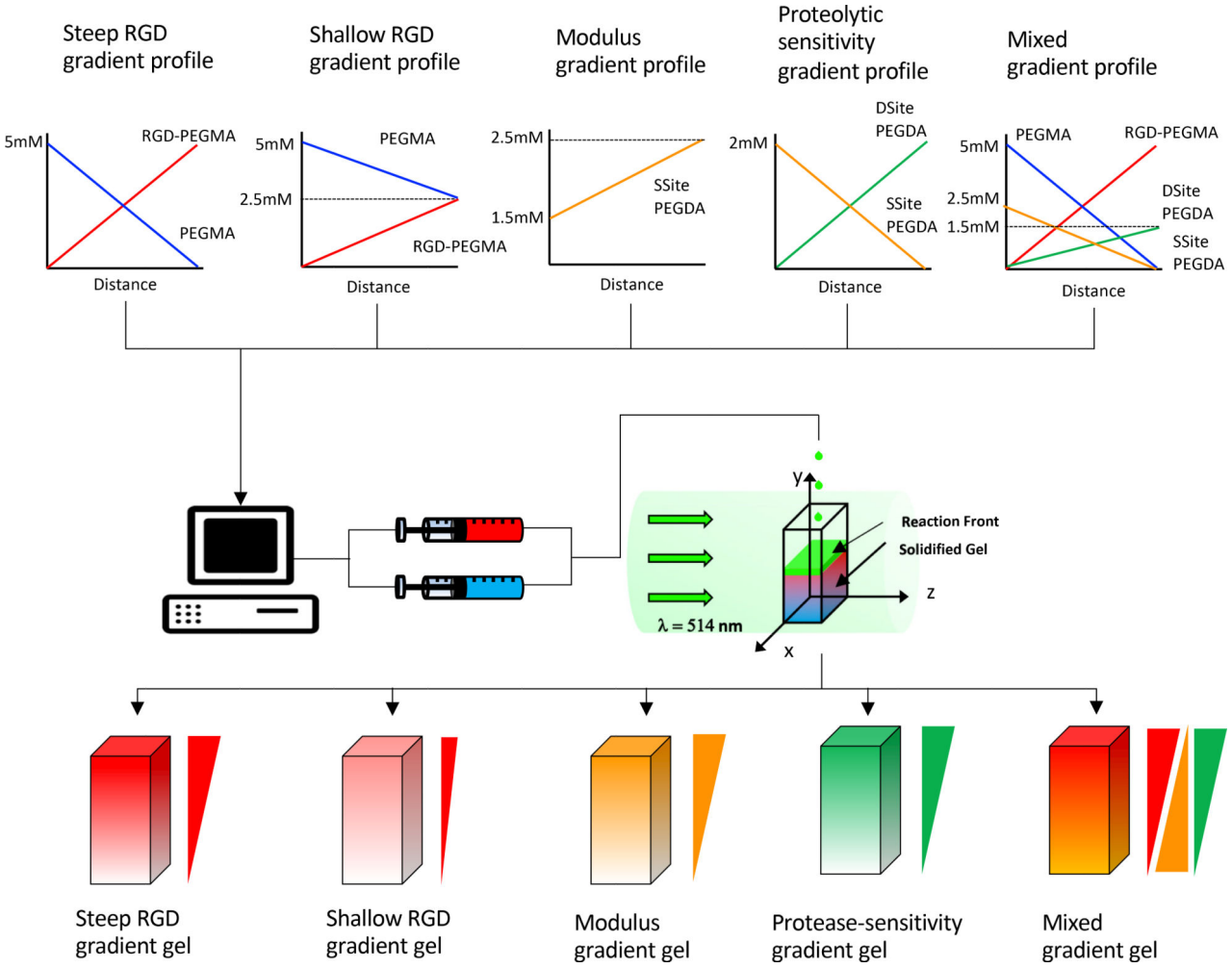

Figure 1:

Schematic representation of photopolymerization process resulting in the formation of hydrogel scaffolds presenting different types of gradients. Spatial gradient of photopolymerizable macromers, RGD-PEGMA, PEGMA, Ssite and Dsite PEGDA were designed for each investigated gradient hydrogel. Syringe pumps were programmed to deliver two distinct precursor solutions into a transparent reaction chamber which was exposed to a visible light ($\lambda = 514nm$) using an argon ion laser. Hydrogel crosslinking occurred continuously with the ascending reaction front as precursor solutions were fed to the reaction vessel. The resultant scaffolds presented (1) steep and (2) shallow gradients in RGD, (3) gradients in elastic modulus, (4) gradients in protease-sensitivity, and (5) a concurrent RGD and protease-sensitivity gradient and a countercurrent or opposing modulus gradient.

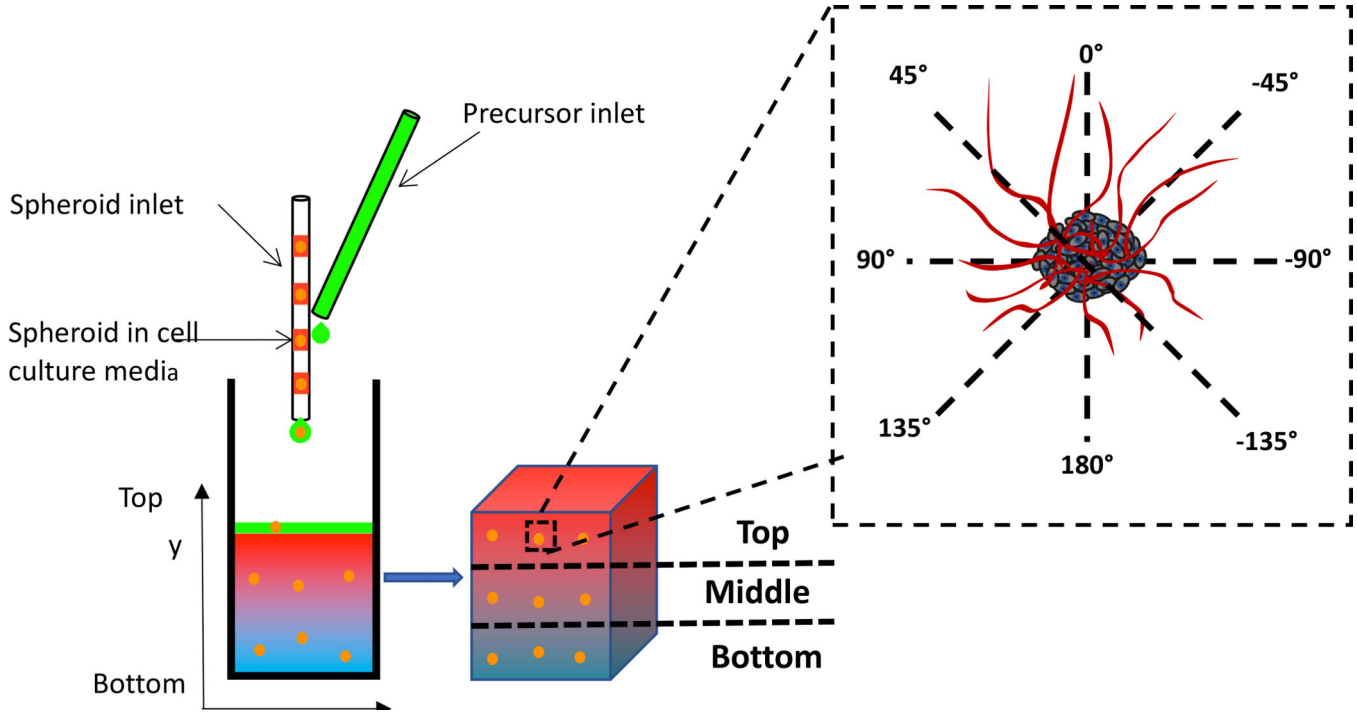

Figure 2:

Schematic of vascular cell-laden gradient spheroid scaffold design and 3D vascular spheroid response to gradients. Prior to hydrogel fabrication, individual spheroids along with 1μL of culture media were pipetted into a glass capillary tube (ID=1 mm) and separated by a small segment of air which prevented spheroid aggregation. Using a syringe pump and a 100μL Hamilton syringe, spheroids were added into the reaction chamber along with the precursor solution and photoencapsulated within gradient hydrogels upon polymerization. The delivery of spheroids was scheduled so that at least three spheroids were spatially photoencapsulated within scaffolds along the gradient(s). Specifically, spheroids were regionally positioned in (1) in the bottom (y=1–3mm), (2) middle (y=4–6mm) and (3) top (y=7–9mm) region of gradient hydrogels. After 7 and 14 days, spheroid sprout lengths were measured along eight different directions where the 0°and 180°represent the directions along the gradient including the top (y=10mm) and bottom regions of the hydrogel (y=0mm), respectively.

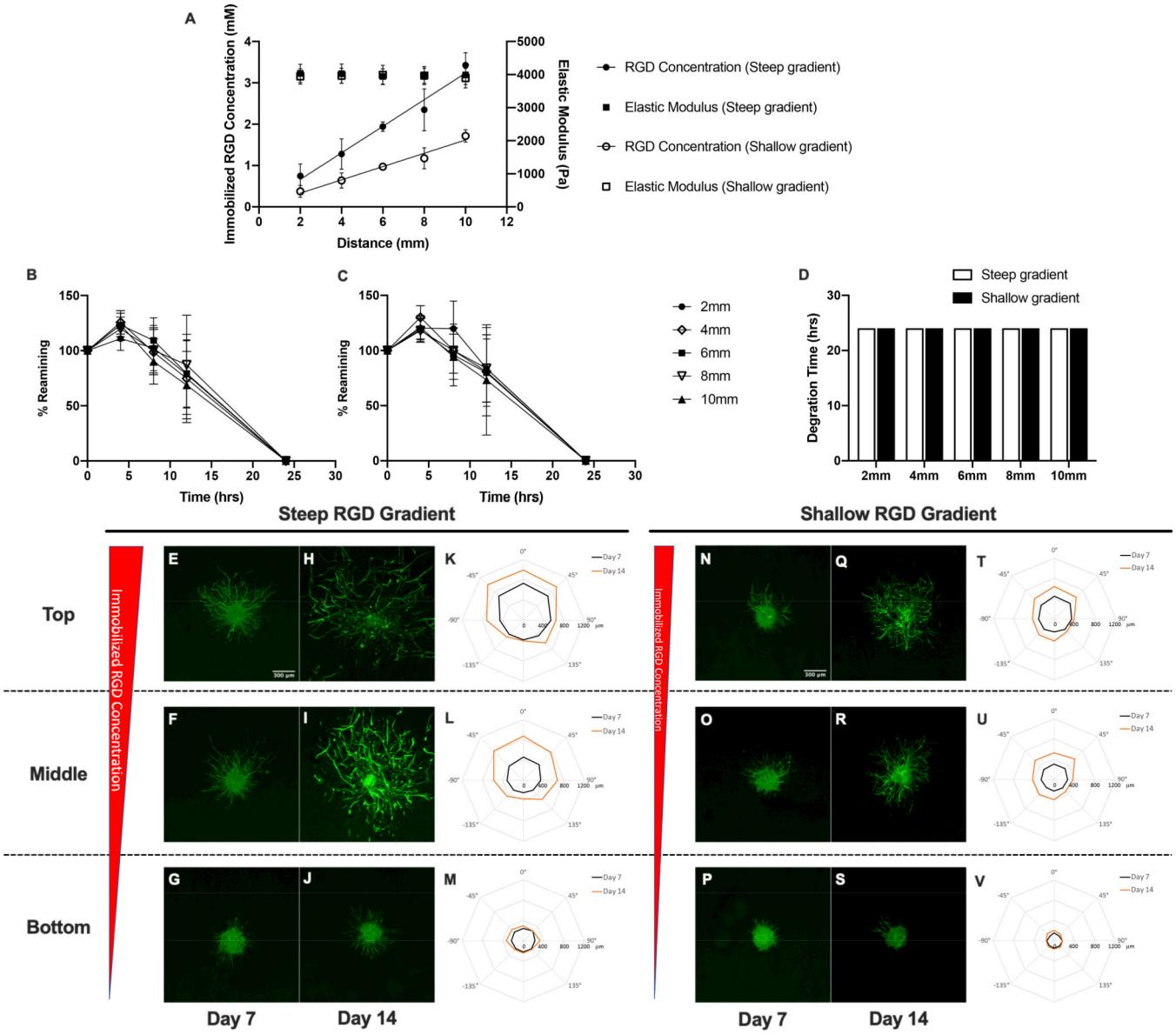

Figure 3:

Characterization of spatial variations in matrix properties and vascular sprout formation in steep and shallow RGD gradient hydrogel scaffolds. (A) Quantification of spatial variations in immobilized RGD concentration and elastic modulus. Degradation kinetics in (B) in steep and (C) shallow RGD gradient hydrogels and (D) time required for complete degradation of RGD gradient hydrogels in collagenase enzyme solution. Confocal images of phalloidin-stained spheroids embedded within top, middle and bottom regions of hydrogel scaffolds with steep (E-J) and shallow (N-S) gradients in immobilized RGD after 7 and 14 day culture. Polar plots of maximum sprout length by angle of spheroids encapsulated in different regions along the gradient (steep RGD (K-M) and shallow RGD (T-V)).

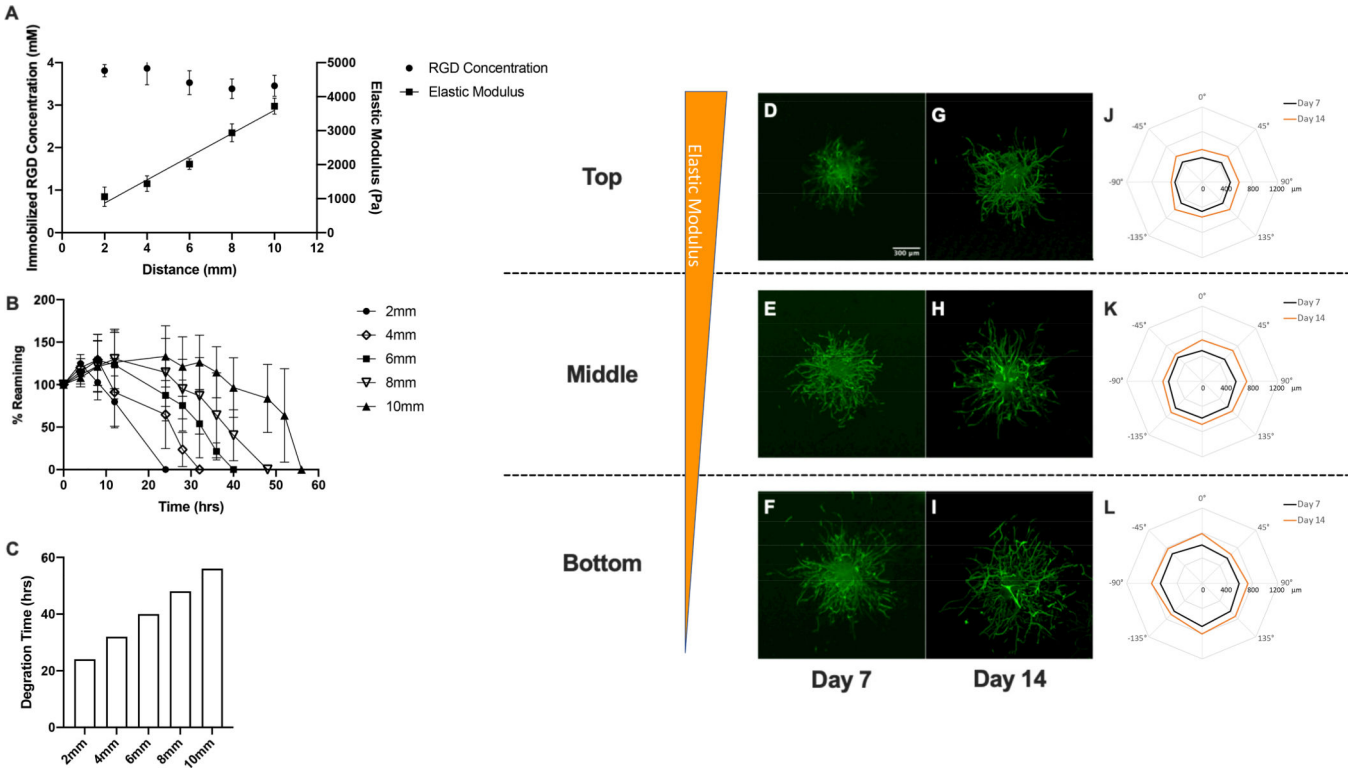

Figure 4:

Characterization of spatial variations in matrix properties and vascular sprout formation in modulus gradient hydrogel scaffolds. (A) Quantification of spatial variations in immobilized RGD concentration and elastic modulus, (B) degradation kinetics and (C) time required for complete degradation in collagenase enzyme solution. Confocal images of phalloidin-stained spheroids embedded within top, middle and bottom regions of hydrogel scaffolds with gradients in elastic modulus after 7 and 14 day culture (D-I). Polar plots of maximum sprout length by angle of spheroids encapsulated in different regions along the gradient (J-L).

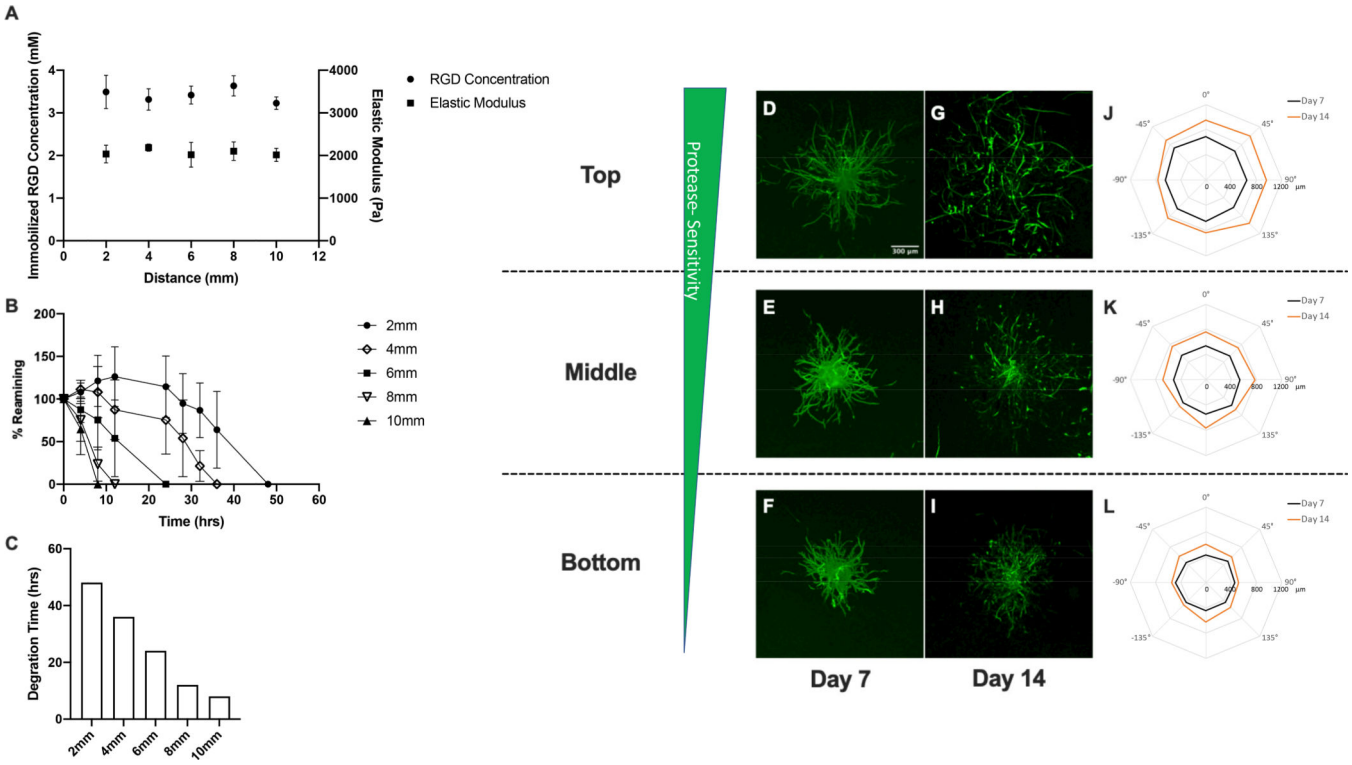

Figure 5:

Characterization of spatial variations in matrix properties and vascular sprout formation in protease-sensitivity gradient hydrogel scaffolds. (A) Quantification of spatial variations in immobilized RGD concentration and elastic modulus, (B) degradation kinetics and (C) time required for complete degradation in collagenase enzyme solution. Confocal images of phalloidin-stained spheroids embedded within top, middle and bottom regions of hydrogel scaffolds with gradients in elastic modulus after 7 and 14 days culture (D-I). Polar plots of maximum sprout length by angle of spheroids encapsulated in different regions along the gradient (J-L).

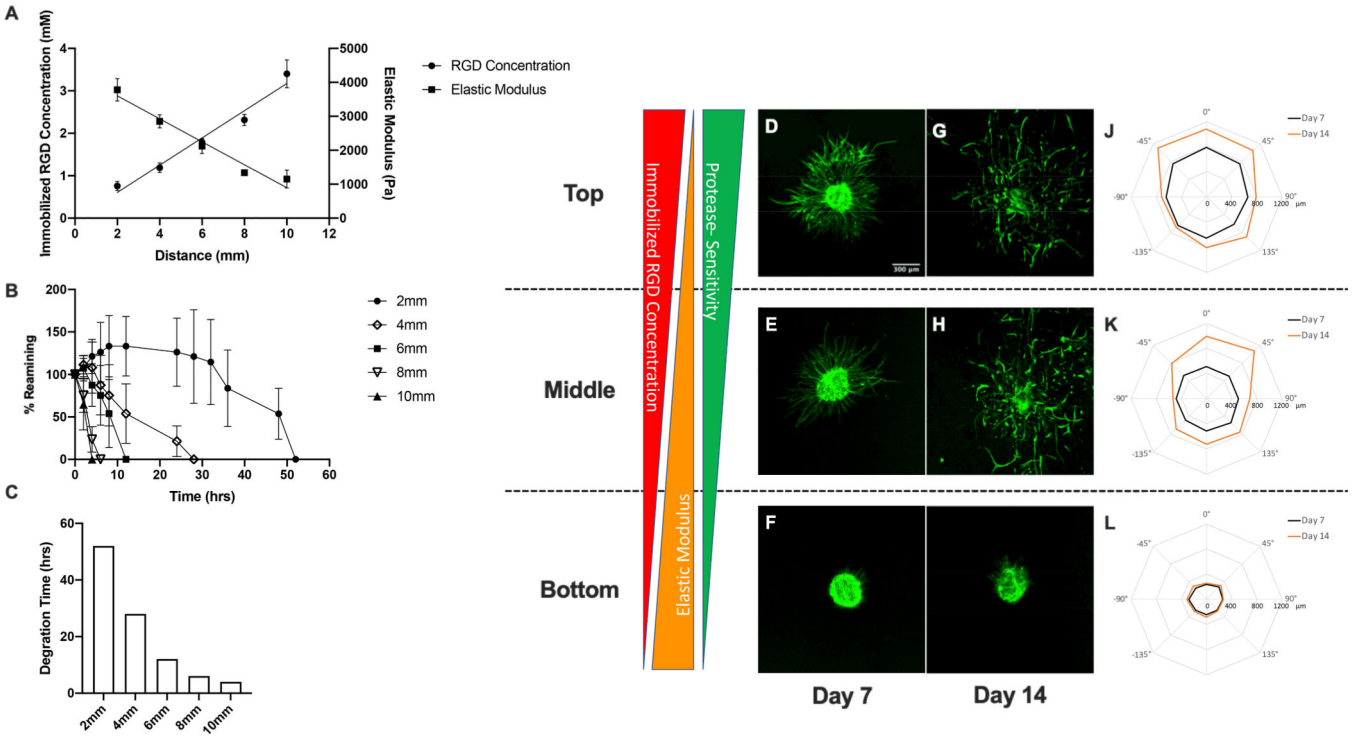

Figure 6:

Characterization of spatial variations in matrix properties and vascular sprout formation in combined gradient hydrogel scaffolds. (A) Quantification of spatial variations in immobilized RGD concentration and elastic modulus, (B) degradation kinetics and (C) time required for complete degradation in collagenase enzyme solution. Confocal images of phalloidin-stained spheroids embedded within top, middle and bottom regions of hydrogel scaffolds with gradients in elastic modulus after 7 and 14 day culture (D-I). Polar plots of maximum sprout length by angle of spheroids encapsulated in different regions along the gradient (J-L).

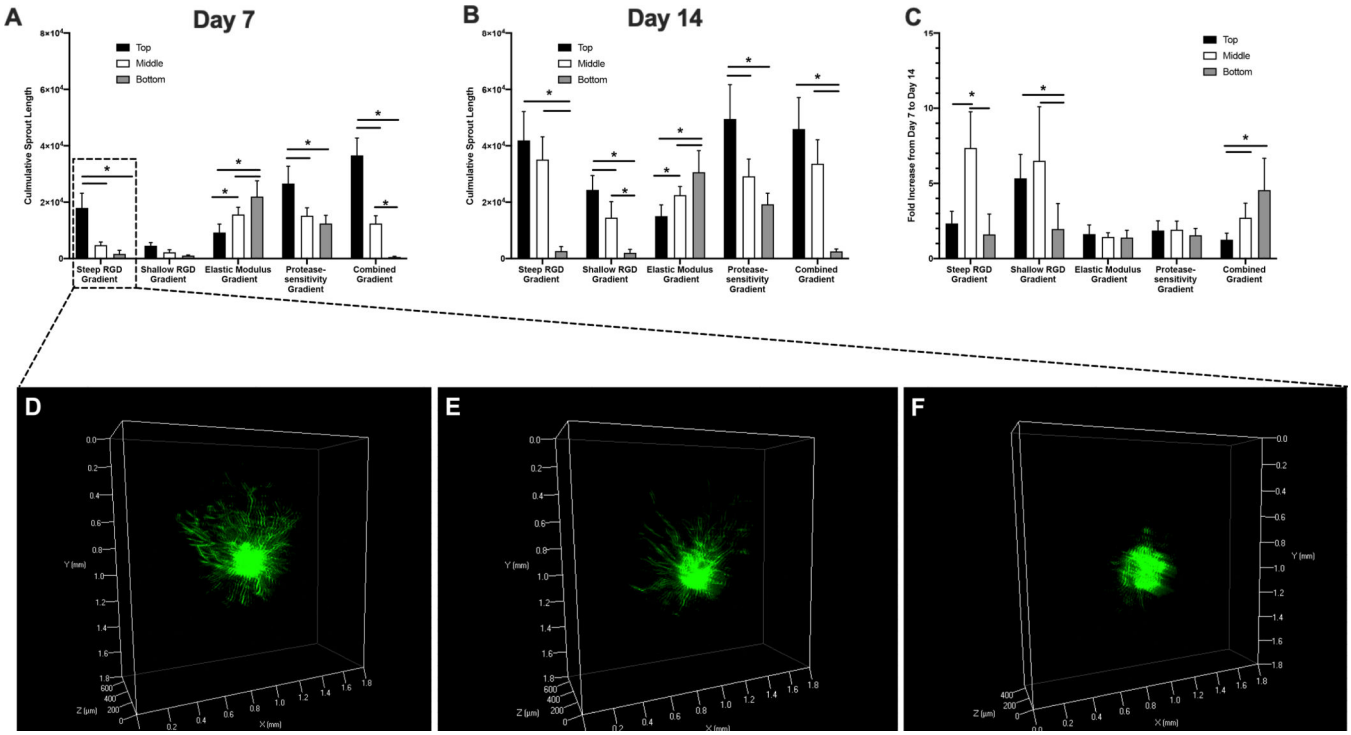

Figure 7:

Total cumulative sprout length of vascular sprout formation in response to imposed gradients after 7 days (A), 14 days (B) and fold increase from day 7 to day 14 (C). 3D volume rendering of phalloidin-stained spheroids encapsulated in top (D), middle (E) and bottom (F) regions of steep RGD gradient hydrogel at day 7. Error bars represent standard deviation. Asterisks (*) indicate statistical significance with $p < 0.05$ (n=3).

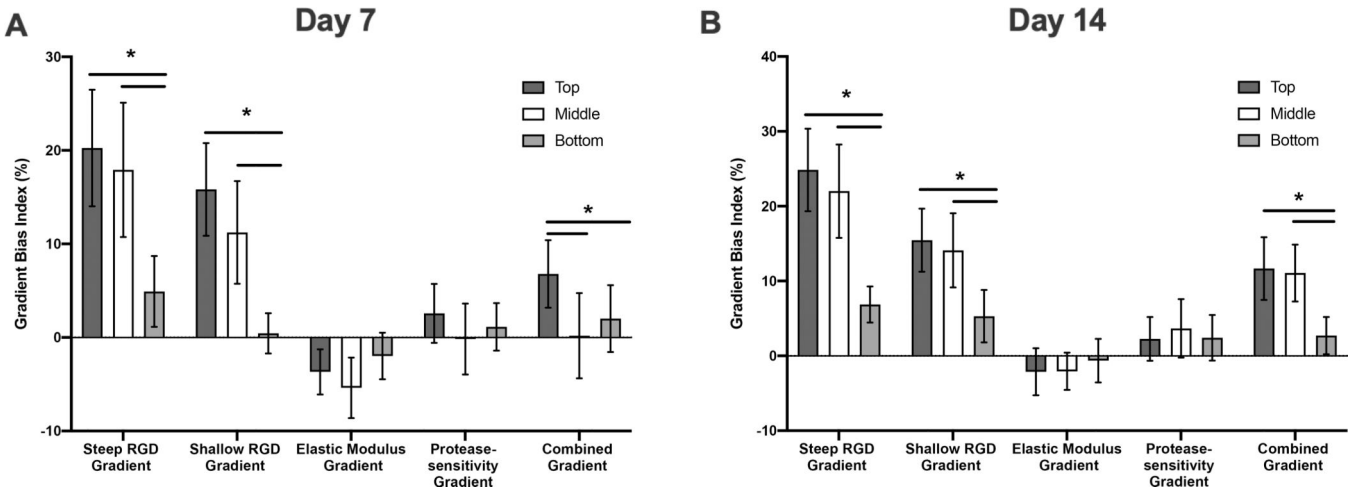

Figure 8:

Gradient bias index of vascular sprout formation in response to imposed gradients at days 7 (A) and 14 (B). Error bars represent 95% confidence interval. Asterisks (*) indicate statistical significance with $p < 0.05$ (n=3).